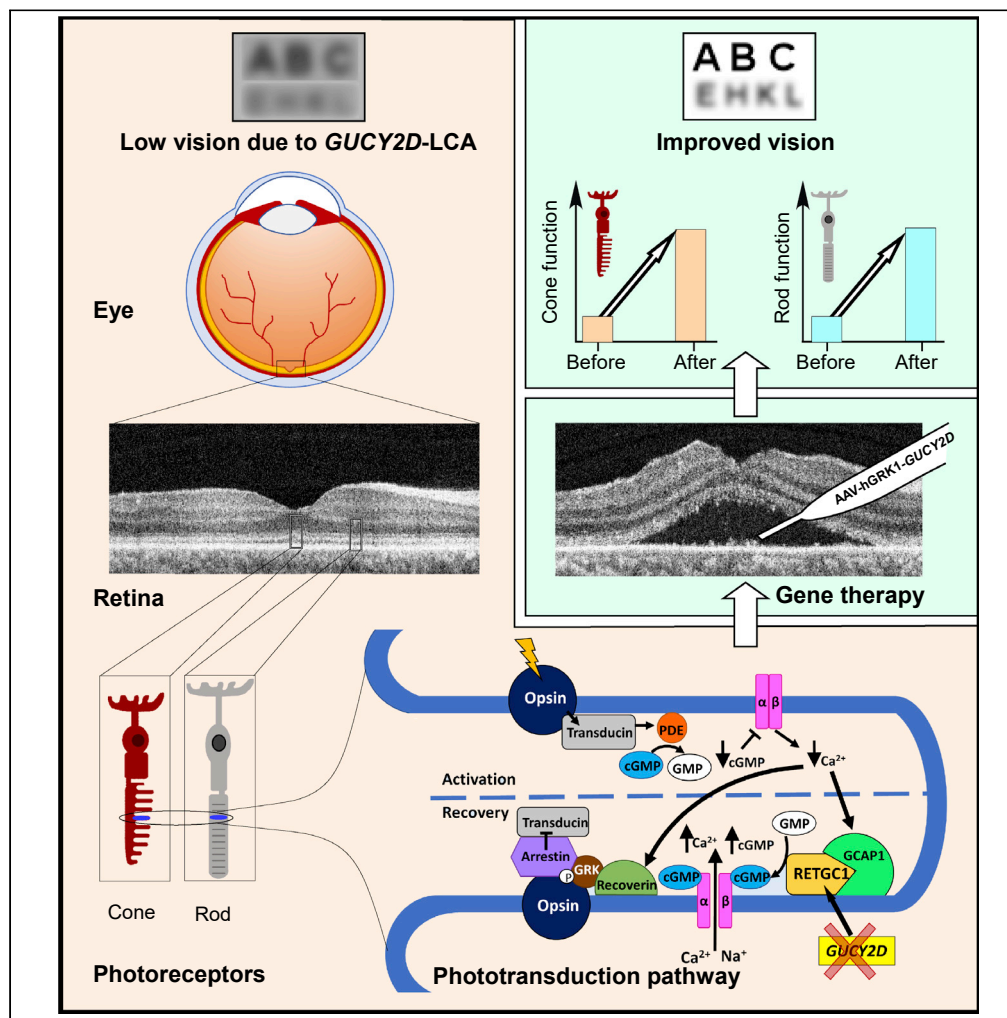## Article

Safety and improved efficacy signals following gene therapy in childhood blindness caused by *GUCY2D* mutations

Samuel G. Jacobson, Artur V. Cideciyan, Allen C. Ho, ..., Sanford L. Boye, Alexander M. Dizhoor, Shannon E. Boye

jacobsos@pennmedicine.upenn.edu

Highlights

Blindness from genetic disorders of the retina has been incurable for centuries

The first photoreceptor-based childhood blindness (*GUCY2D*-LCA) has now been treated

Proof of safety and efficacy of subretinal gene therapy in *GUCY2D*-LCA is reported

iScience

Article

Safety and improved efficacy signals following gene therapy in childhood blindness caused by *GUCY2D* mutations

Samuel G. Jacobson,[1,7,*] Artur V. Cideciyan,[1] Allen C. Ho,[2] Igor V. Peshenko,[3] Alexandra V. Garafalo,[1] Alejandro J. Roman,[1] Alexander Sumaroka,[1] Vivian Wu,[1] Arun K. Krishnan,[1] Rebecca Sheplock,[1] Bee-Lin Cheang,[4] Vanessa Davidson,[4] Catherine R. O'Riordan,[4] Sanford L. Boye,[5] Alexander M. Dizhoor,[3] and Shannon E. Boye[6]

SUMMARY

A first-in-human clinical trial of gene therapy in Leber congenital amaurosis due to mutations in the *GUCY2D* gene is underway, and early results are summarized. A recombinant adeno-associated virus serotype 5 (rAAV5) vector carrying the human *GUCY2D* gene was delivered by subretinal injection to one eye in three adult patients with severe visual loss, nystagmus, but preserved retinal structure. Safety and efficacy parameters were monitored for 9 months post-operatively. No systemic toxicity was detected; there were no serious adverse events, and ocular adverse events resolved. P1 and P2 showed statistically significant rod photoreceptor vision improvement by full-field stimulus testing in the treated eye. P1 also showed improvement in pupillary responses. Visual acuity remained stable from baseline in P1 and P2. P3, however, showed a gain of 0.3 logMAR in the treated eye, indicating greater cone-photoreceptor function. The results show safety and both rod- and cone-mediated efficacy of this therapy.

INTRODUCTION

Childhood blindness from retinal disease, clinically grouped as Leber congenital amaurosis (LCA), is caused by mutations in more than 25 genes (Kumaran et al., 2018). Three of these molecular subtypes of LCA have been early targets for gene-specific therapies because of evidence for potential improvement in vision (Cideciyan and Jacobson, 2019). Dissociation of photoreceptor structure and function is one of the keys to candidacy. In clinical trials of two subtypes, *RPE65*- and *CEP290*-LCA, there was evidence of safety and efficacy (Cideciyan et al., 2008, 2019; Bainbridge et al., 2008; Maguire et al., 2008; Jacobson et al., 2012). Clinical trial results for the remaining candidate, LCA caused by *GUCY2D* mutations, have not been reported to date.

Disease mechanisms of the three molecular forms of LCA differ. *RPE65*-LCA is a retinoid cycle disease of the retinal pigment epithelium (RPE); gene augmentation led to dramatic changes within days of treatment mostly in rod photoreceptor-mediated vision as vitamin A became available to the treated region of the retina. There were also improvements in extra-foveal cone vision. *CEP290*-LCA is a photoreceptor ciliopathy, and the human disease causes early loss of rod photoreceptors but leaves an intact central island of cone photoreceptors (Cideciyan et al., 2007, 2011, 2019; Jacobson et al., 2017a, 2017b). Cone photoreceptor-mediated vision improved within a month after an antisense oligonucleotide intravitreal injection (Cideciyan et al., 2019).

A human *GUCY2D* gene codes for retinal guanylyl cyclase isozyme-1, RetGC1 (Dizhoor et al., 1994; Lowe et al., 1995). A spectrum of retinal disease is associated with mutations in the *GUCY2D* gene, including autosomal dominantly inherited cone-rod and cone degenerations and autosomal recessive LCA. *GUCY2D* is one of the major causes of LCA (Sharon et al., 2018). *GUCY2D*-LCA is due to the insufficient rate of cGMP production, incapable of maintaining the normal photocurrent in both rods and cones (Boye, 2014). Patients can manifest more cone than rod dysfunction, more rod than cone dysfunction, or equal losses. A key feature in *GUCY2D*-LCA is that despite severe rod and cone dysfunction, there is relatively preserved photoreceptor integrity (Cideciyan and Jacobson, 2019; Jacobson et al., 2013, 2017a, 2017b). A treatment trial in *GUCY2D*-LCA could thus lead to improvements in rod- or cone-mediated vision, or both.

[1]Scheie Eye Institute, Department of Ophthalmology, Perelman School of Medicine, University of Pennsylvania, Philadelphia, PA, USA

[2]Wills Eye Hospital, Thomas Jefferson University, Philadelphia, PA, USA

[3]Pennsylvania College of Optometry, Salus University, Elkins Park, PA, USA

[4]Genomic Medicine Unit and US Regulatory Affairs, Sanofi, MA, USA

[5]Department of Pediatrics, Powell Gene Therapy Center, University of Florida College of Medicine, Gainesville, FL, USA

[6]Department of Pediatrics, Division of Cellular and Molecular Therapy, University of Florida College of Medicine, Gainesville, FL, USA

[7]Lead contact

*Correspondence: jacobsos@pennmedicine.upenn.edu

https://doi.org/10.1016/j.isci.2021.102409

Table 1. Clinical trial of gene therapy for *GUCY2D*-LCA

Age at baseline (y)/Sex	*GUCY2D* mutations Allele 1/Allele 2	Treated Eye	Injection site[a]	Concentration (vg/mL)	Total volume[b] (µL)	Entry VA, (logMAR)[c] Study eye	Entry VA, (logMAR)[c] Control eye	Entry FST (log10)[d] Study eye	Entry FST (log10)[d] Control eye
P1 45/F	c.2943delG, p.Ser981del1bp[e,f]/ c.2302C>T, p.Arg768Trp[e,f,g]	Right	Macula	3.3×10^{10}	300	2.6	2.6	4.3	4.5
P2 35/M	c.1780_1783delCTCT, p.Leu594Thrfs*42[f]/ c.3160T>A, p.Phe1054Ile[f]	Right	Superior retina	3.3×10^{10}	200	1.25	1.19	4.4	4.2
P3 23/F	c.1978C>T, p.Arg660*[h]/ c.2984G>A, p.Arg995Gln[i]	Left	Macula	3.3×10^{10}	300	1.27	0.65	5.2	5.3

[a]Planned for the macula; the bleb in P2 was unable to be raised in the macula and was in the superior retina instead.

[b]Intended subretinal volume was 300 µL, but P2 received approximately 200 µL, the estimate at time of surgery.

[c]Best-corrected visual acuity at baseline visit, measured from back-lit Early Treatment Diabetic Retinopathy Study charts adjusted for distance (0.00 logMAR = 20/20 Snellen VA at 4 m) in P2 and P3; BVRT (Berkeley Rudimentary Vision Test) was used for P1.

[d]Rod sensitivity (in log10 1/(phot-cd.m-2)) at baseline visit, measured by full-field stimulus testing (FST) with blue stimulus.

[e]Jacobson et al. (2013).

[f]Jacobson et al. (2017b).

[g]Hanein et al. (2004).

[h]Li et al. (2009).

[i]Novel.

In the present study, three patients with *GUCY2D*-LCA were treated in a first-in-human gene augmentation clinical trial and followed for 9 months post-therapy. There was an acceptable safety profile and preliminary evidence of vision improvement. These early results provide guideposts for conducting ongoing and future trials in *GUCY2D*-LCA.

RESULTS

A non-randomized Phase I/II single center, open-label safety and efficacy study of uniocular subretinally injected AAV5-*GUCY2D* (Figure S5) in patients with LCA caused by biallelic mutations in the *GUCY2D* gene is ongoing (ClinicalTrials.gov Identifier: NCT03920007). Upon observing substantial rod and cone improvements, we decided to perform an interim analysis of the results from the first three patients (P1, female, 45 years old; P2, male, 35 years old; and P3, female, 23 years old) to receive treatment. These Cohort 1 patients were administered the lowest dose planned within the trial. All patients were compound heterozygotes for disease-causing mutations in the *GUCY2D* gene (Table 1).

GUCY2D mutant alleles *in vitro* did not code for an active enzyme with one exception

In all three patients, one of the two LCA alleles harbored a mutation (either a missense or a frameshift/truncation) in the catalytic domain of the enzyme, and the other, in a kinase homology domain. Only in P1, products of both alleles retained the dimerization and the catalytic domains of the cyclase, whereas in P2 and P3 one of the alleles would be *a priori* unable to produce catalytically active enzyme (see Figure S1). Those RetGC1 mutants that could possibly possess catalytic activity were expressed in HEK293 cells and assayed in the presence of the photoreceptor-specific guanylyl cyclase-activating protein, Mg^{2+} GCAP1 (Figure 1) (Palczewski et al., 1994; Dizhoor et al., 2010). None of the *GUCY2D* alleles in P1 and P2 coded for an active enzyme. For one allele (p.Arg955Gln) of P3, however, traces of guanylyl cyclase activity were detectable (Figure 1B). Co-expression of the two LCA alleles in P1 also failed to produce an active enzyme (see Figure S1E).

Human phenotype of the patients with *GUCY2D*-LCA shows rod and cone photoreceptor dysfunction to different degrees pre-treatment

Visual acuity was severely impaired (worse than 1.0 logMAR in the study eyes) with nystagmus from early life. Rod photoreceptor-mediated sensitivities measured by FST (full-field stimulus test) were abnormally
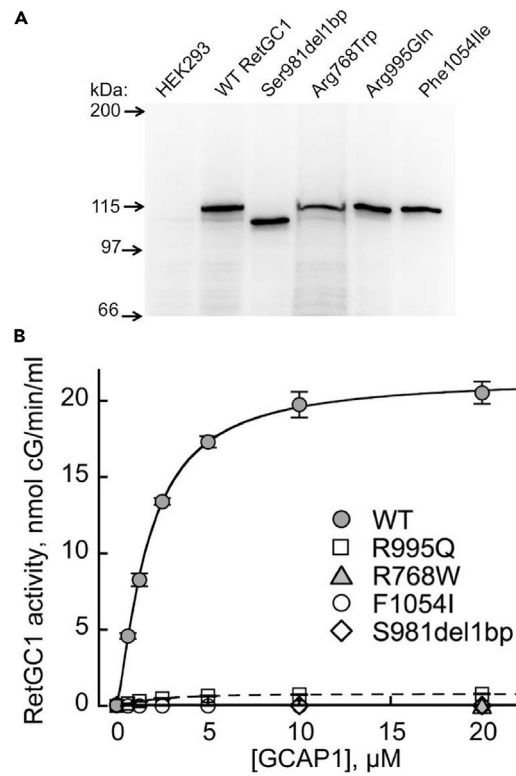
Figure 1. Loss of the activity in RetGC1 variants coded by *GUCY2D* LCA alleles in the patients

(A) Western immunoblotting of HEK293 cell membranes expressing RetGC1 variants harboring amino acid substitutions coded by the *GUCY2D* LCA alleles; probed by anti-RetGC1 antibody.

(B) The guanylyl cyclase activity of RetGC1 (mean average $\pm$ SD, from 2 to 4 independent measurements) using different preparations of HEK293 membranes reconstituted with Mg^{2+} GCAP1; wild type ($\bullet$), Arg768Trp ($\blacktriangle$), Ser981del1bp ($\diamond$), Arg995Gln ($\square$), and Phe1054Ile ($\bigcirc$); the activities of RetGC1 in each case were corrected by the levels of their expression relative to wild type.

reduced by ~0.7–1.8 log units (l.u.) from the normal mean of 6.03 $\log_{10}$ 1/(phot-cd.m^{-2}) (2SD = $\pm$0.6; n = 9, ages 22–58) (Table 1) (Jacobson et al., 2013; Roman et al., 2007; Csaky et al., 2008).

Are there photoreceptor structural abnormalities in these patients? Cross-sectional retinal imaging with optical coherence tomography (OCT) across the horizontal meridian of the patients through the fovea was compared with that of normal (Figure 2). The patients represent a spectrum of foveal ONL (outer nuclear layer) loss. P1 had the most profound foveal ONL thinning (8.2 μm versus normal average thickness of 98 μm, 2SD = 21.5 μm). P2 had foveal ONL of 43 μm; and P3 had 79 μm, which is within normal limits (Figures 2B–2D). ONL eccentric to the fovea was generally retained; at 10° in the nasal retina, for example, P1, P2, and P3 had 49.1, 53.8, and 54.5 μm thickness, all of which are within normal limits (average 55.7 μm, 2SD = 11.5 μm). Quantitation of the ONL illustrates the differences between the patients (Figure 2E). The rod:cone ratio across this expanse of central retina illustrates that central cell loss is mainly a loss of cone nuclei, whereas outside the foveal region, the patients have ONL thickness that is within normal limits. These extrafoveal areas are rod-dominated, attaining rod:cone ratios of 20:1 (Figure 2F).

Systemic and ocular parameters indicate an acceptable safety profile of the therapy

The patients underwent retinal surgery (including vitrectomy and subretinal injection of vector) (Hauswirth et al., 2008) in one eye and were evaluated post-operatively with complete eye examinations, general physical examinations, and laboratory tests (see Table S1 for study schedule). Physical examinations were unchanged from baseline, and no clinically significant abnormalities were detected in hematology, serum chemistry, coagulation parameters, and urinalysis after retinal gene transfer. Ocular adverse events (AEs) shared by all patients post-operatively were in the treated eyes (and all resolved): some discomfort,
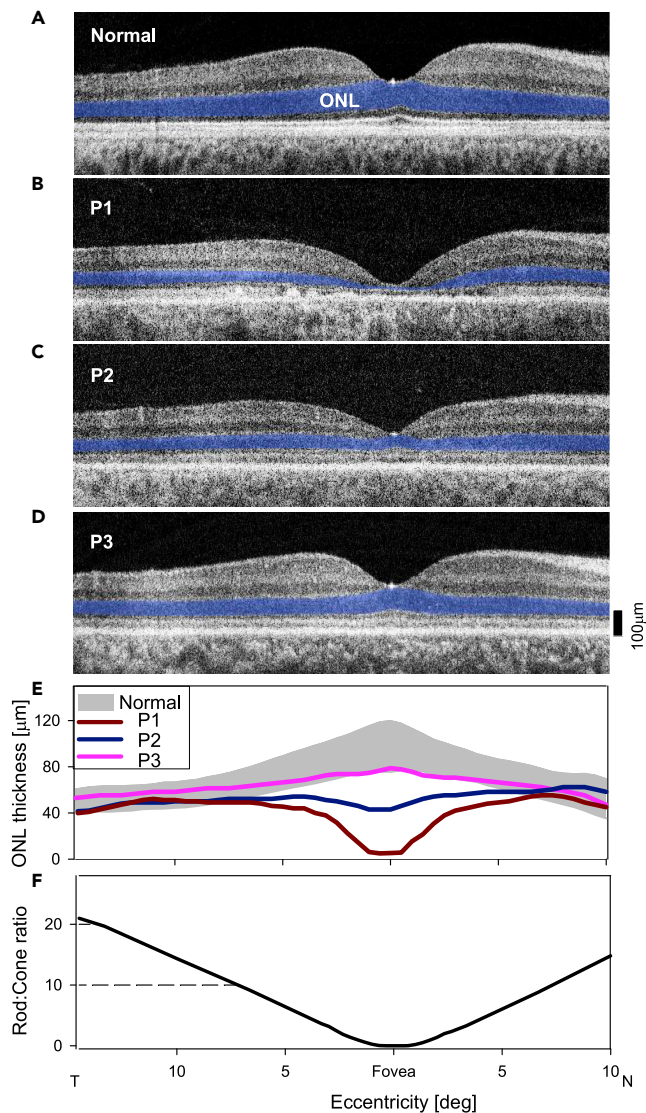
Figure 2. Photoreceptor structural disease in the patients with *GUCY2D*-LCA compared with normal

(A–D) OCT scans across the horizontal meridian through the fovea in a normal subject, and in P1–P3. ONL, photoreceptor outer nuclear layer, is highlighted in blue for visibility.

(E) Quantitation of the ONL in the patients compared with normal limits (gray bar; mean ±2SD; n = 12, ages 8–48 years; Jacobson et al., 2013) further illustrates the depressed foveal ONL in P1 and less so in P2. In P3, ONL is within the lower limits of normal.

(F) Ratio of rods to cones across the scanned retinal area emphasizes that outside the cone-dense fovea, rods become the dominant photoreceptor population.

subconjunctival hemorrhage, and reduced intraocular pressure (see Table S2). P3 showed other surgery-related AEs: minimal increase in vitreous cellularity (prompting use of oral steroids for 8 days post-operatively, which was 6 days longer than by the protocol), then steroid-induced ocular hypertension (leading to discontinuation of steroids and use of a topical antiglaucoma medication for 5 days), and a retinal hole noted at surgery and treated with intraoperative laser. All AEs in P3 were resolved within 14 days.

We asked if there was any evidence of retinal damage from the surgical procedure, specifically in the region of the induced retinal detachment (i.e., bleb). OCT scans were recorded before and at five visits after surgery spanning 1 month to 9 months post-operatively (Figure S2). The site and extent of the injection are drawn on near-infrared fundus images of the treated eyes (OD in P1, OD in P2, and OS in P3). Despite

difficulties of recording such images due to nystagmus, scans were able to be performed and quantified. P1's bleb was in the macula and sampling of photoreceptor laminar thicknesses (ONL, IS [inner segment], and OS [outer segment]) were at 10° in the temporal retina. P2's bleb was not able to be placed in the macula, and the therapeutic vector was delivered (with lesser volume, Table 1) in the superior retina (see Figure S2). Measurements of ONL, IS, and OS thicknesses were at 28° superiorly. P3's bleb was in the macula; the importance of foveal ONL in this patient led to sampling at the fovea. All measurements made after injection in the treated eye (compared with baseline and with the untreated eye) did not reveal any loss of photoreceptor laminar thickness at the loci sampled in each patient (see Figure S2).

Rod photoreceptor-mediated vision improves post-therapy in P1 and P2

Visual sensitivities to chromatic stimuli in the dark-adapted state at baseline and for 9 months after uniocular gene therapy were measured in treated and untreated eyes of all patients. Common to all three patients, treated eyes immediately after surgery had abnormally reduced FST sensitivities relative to baseline (reductions ranged from 0.2 to 1.0 l.u. during the first week after surgery). By 30–60 days post-operatively, baseline levels were regained in treated eyes of P2 and P3, whereas an improvement was already evident in P1 (Figure 3). P1 showed functional improvements in excess of 1 l.u. in the treated eye at all post-operative visits from 30–270 days (median 1.34, range 1–1.4 l.u., p < 0.01). Objective pupillary light responses also improved in the treated eye of P1 (see Figure S3). P2 showed a lesser perceptual efficacy signal that appeared to be delayed until the 60-day time point, but then increased steadily over subsequent visits (median of visits from 60–270 days, 0.59, range 0.33–0.78 l.u.). P3 showed no post-operative improvement by FST (median 0.06, range −0.1 to 0.15 l.u.) (Figure 3A). Objective pupillary light responses of P2 and P3 did not demonstrate improvements (see Figure S3).

There can be some visit-to-visit long-term fluctuation in the perceptual judgments made by subjects, and some fluctuations were apparent in the sensitivities recorded in untreated eyes of patients (Figure 3A). Examination of differences between eyes can account for these fluctuations. The interocular differences of perceptual FST sensitivities related to baseline (Figure 3B, green arrows and asterisks) were statistically significant for all post-operative visits of P1 (post-operative mean 0.97 l.u., p < 0.01) and most of the visits of P2 (post-operative mean 0.48 l.u.; p=<0.01 for all except for day 89 where it was not significant, p = 0.13).

Results of short- (blue) and long- (red) wavelength sensitivity changes from baseline are both plotted (Figure 3B), and the photoreceptor mediation of these responses are shown (Figure 3C). In all patients at all time points, the FST responses were rod photoreceptor-mediated.

Improvement in visual acuity post-therapy in P3

Visual acuity, a conventional assay of efficacy in clinical trials of ocular disease (Ferris et al., 1982), is severely reduced in *GUCY2D*-LCA (Jacobson et al., 2013, 2017b). The inclusion criterion was that visual acuity could be no better than 20/200 (1.0 logMAR) in the eye to be treated. Best-corrected acuities were able to be measured in P2 and P3 using ETDRS (Early Treatment of Diabetic Retinopathy) and E charts. P1 had light perception (LP) vision only and was unable to read ETDRS letters or see the direction of the tumbling E; low vision BVRT (Berkeley Rudimentary Vision Test) gratings were used instead (Bailey and Lovie-Kitchin 2013). The acuity task was challenging for P1, and there was variability of results throughout the trial; in addition to wandering eye movements, there was bilateral loss of foveal outer retinal structure (Figure 2B). Before surgery, the average of screening (2.3) and baseline (2.9) results was 2.6 logMAR in each eye. Thereafter for 9 months, both eyes were most often at 2.3 logMAR than any other value (Figure 4A). Clinically, the patient remained LP throughout the trial. P2 had measurable acuities of 1.19 logMAR in the right eye and 1.25 in the left eye at baseline. There was no major improvement or decrement in acuities in the two eyes over the 9 months of observation. P3 had asymmetry of visual acuities; the eye with worse acuity is conventionally chosen for the subretinal injection, and this was the left eye in P3. By day 32, there was an improvement in acuity of this eye above baseline by about 0.3 logMAR, and this persisted for the 270 days post-treatment. At 9 months, the acuity of the treated eye was significantly different than baseline (Figure 4B). The untreated eye remained at baseline levels. This degree of change in the treated eye has been considered a conservative estimate of clinically significant improvement (Sieving et al., 2006).

Was the improved visual acuity evidence of cone photoreceptor-mediated efficacy? The final visual acuity in P3's treated eye cannot be definitively attributed to cone or rod mediation (Hecht, 1927; Lamb, 2016;
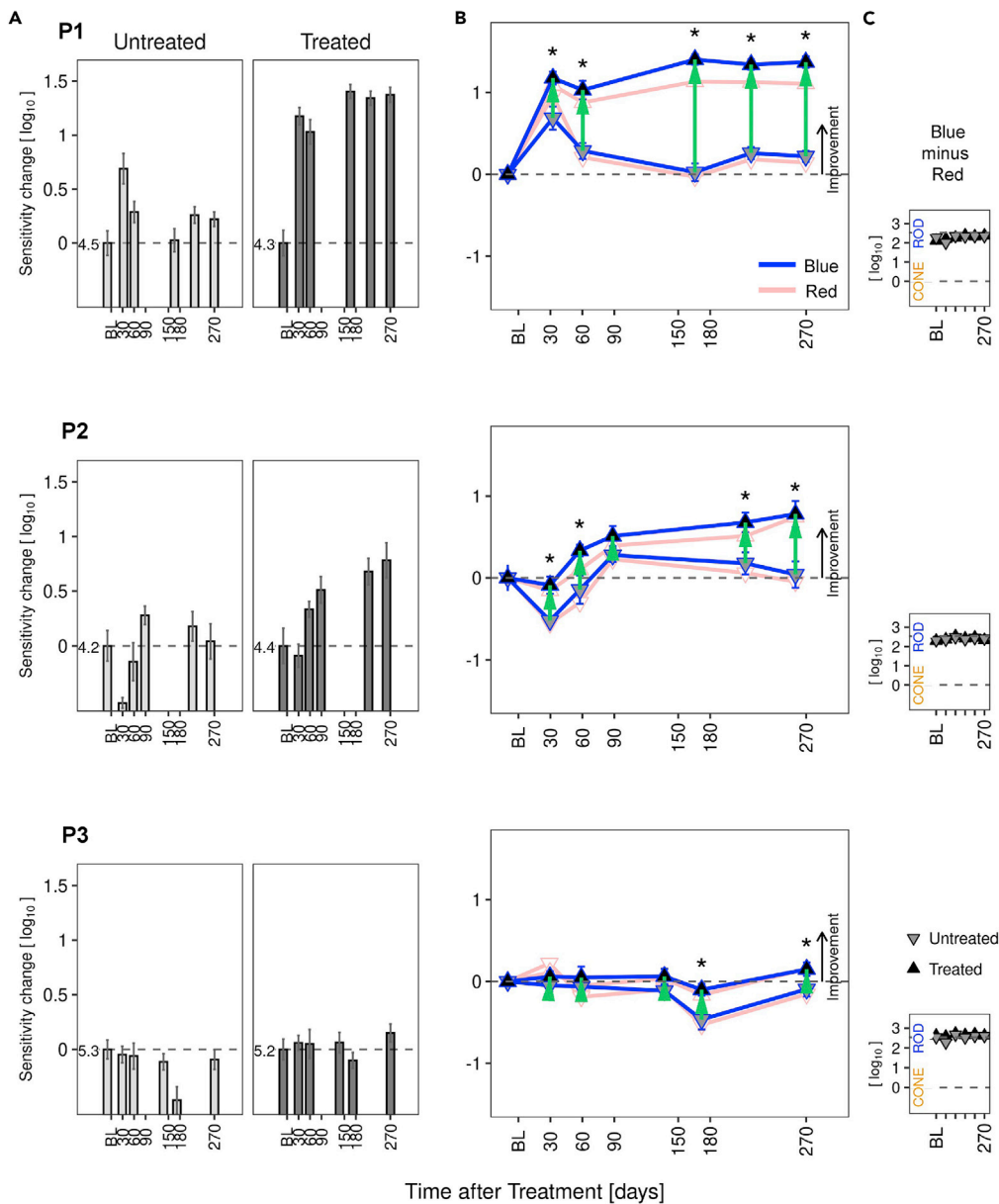
Figure 3. Rod-mediated vision improves in treated eyes of patients with *GUCY2D*-LCA.

Dark-adapted chromatic full-field stimulus test (FST) results in P1, P2, and P3.

(A) Sensitivity changes from baseline for the short-wavelength stimulus, shown separately for untreated and treated eyes. In the treated eye, P1 had improvements greater than 1.0 log unit at all post-operative visits; P2 reached 0.78 l.u. at the last visit. P3 did not show improvement. Sensitivity levels at baseline are indicated in $\log_{10}(1/cd.m^{-2})$ to the left of the zero-change dashed line.

(B) Change in sensitivity from baseline in treated (up-triangles) and untreated (down-triangles) eyes for the photopically matched targets (blue and red lines, respectively for short and long wavelength). Localization of up-triangles above down-triangles indicates a post-treatment improvement of the treated eye relative to the untreated eye. Green arrows indicate interocular differences with respect to baseline; there is an asterisk when significantly different than zero ($\alpha = 0.05$, eye/visit interaction term in a linear model).

(C) Chromatic difference between sensitivities to the two targets (short-minus long-wavelength, blue minus red). Differences near 2.54 $\log_{10}$ indicate rod mediation (rods detecting both colors); values near zero would imply cone mediation. Rod mediation was observed in both eyes of the three patients at all visits. BL, baseline visit.
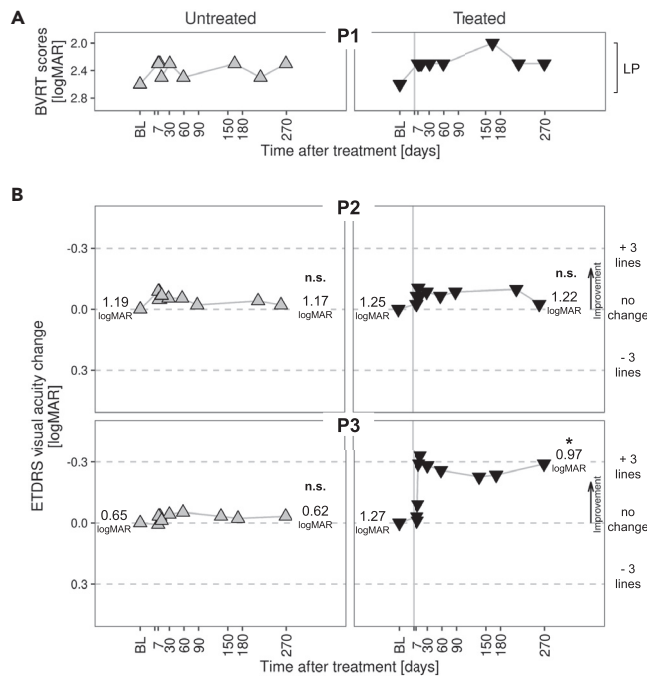
Figure 4. Visual acuities for untreated and treated eyes in the patients

(A) Light perception (LP) vision in P1 did not allow for standard ETDRS visual acuity measures, as in P2 and P3. A low-vision method, BVRT (Berkeley Rudimentary Vision Test) charts, was used instead. Scores from BVRT sessions are plotted.
(B) P2 and P3 had ETDRS (Early Treatment of Diabetic Retinopathy), and tumbling E data collected and visual acuity change from baseline are plotted. Labels on the left and right of each panel indicate the average best-corrected visual acuity at baseline and at month 9, respectively, where formal statistics were performed. Horizontal dashed lines correspond to no change; +3 and −3 ETDRS chart lines for reference. Change of one line in the ETDRS chart corresponds to 0.1 logMAR. Symbols: up-triangles, untreated eye results; down-triangles, treated eye results. The vertical line at day 0 of Treated Eye graphs represents the day of surgery. Post-operative reduction in acuity of the treated eye occurred in all patients (not plotted) but then recovered to baseline by day 7. *, Mean at last visit significantly different than at baseline (two sample, two-tailed t test, α = 0.05); n.s., difference not significant.

Foote et al., 2018). The question of cone versus rod mediation was asked informally at baseline and post-treatment visits when assessing fixation stability with a microperimeter (Cideciyan et al., 2009; Luo et al., 2015). The red fixation target for the task was consistently described by the patient as red or orange with either eye, suggesting that there was color perception mediated by L/M (long/medium wavelength-sensitive) cone photoreceptors. Cone sensitivity was formally measured in each eye at baseline, 30 days, and after 270 days post-treatment using light-adapted static perimetry profiles across the central visual field (see Figure S4) (Roman et al., 2005; Matsui et al., 2015; Jacobson et al., 2016). P3 was the only patient with sufficient fixation to perform this test. Both eyes, compared with normal, were reduced to a central island only, but the asymmetry of function in the two eyes at baseline was evident with the untreated eye showing higher peak sensitivity than the eye later treated (see Figure S4A). Baseline and 32-day post-operative profiles in the untreated eye were nearly identical; the treated eye at 32 days, however, had higher sensitivity at fixation and at nearby loci within the island than at baseline. At 270 days post-operatively, the untreated eye remained the same as at baseline. The treated eye continued to show a positive difference from baseline (see Figure S4B). Average sensitivity change within 40° of field at baseline versus two post-operative visits for untreated and treated eyes is shown graphically for light-adapted cone function (see Figure S4C, left panel). The interocular differences related to baseline were statistically significant for the post-operative visits (p < 0.01 and p = 0.025 for 32 and 270 days, respectively). Perimetric and visual acuity results taken together imply increased cone photoreceptor function at the locus of fixation with treatment. Dark-adapted chromatic perimetric profiles were also performed at these visits, and there was also a difference between untreated and treated eyes (see Figure S4C, right panel, p = 0.02 and p = 0.023 for 32 and 270 days, respectively) suggesting improvement of parafoveal rod-mediated function after treatment.

DISCUSSION

More than a century of basic research has led to detailed understanding of the vertebrate phototransduction cycle—the biochemical cascade in rod and cone photoreceptors that occurs when light is absorbed and vision signaling begins. Activation and amplification of the process is followed by deactivation, which allows phototransduction to repeat and vision to continue (Ebrey and Koutalos, 2001; Vinberg et al., 2018). With knowledge of the molecular mechanisms of these early stages of vision came elucidation of many candidate genes for inherited photoreceptor diseases. The *GUCY2D* gene encodes retinal membrane guanylyl cyclase (RetGC1), a key enzyme in the deactivation path of phototransduction. Mutations in *GUCY2D* are now known to be a relatively common cause of the severe childhood-onset autosomal recessive retinal blindness, LCA (Perrault et al., 1996; den Hollander et al., 2008).

Before the current report, there were only two other molecular forms of LCA with evidence of visual improvement in early cohorts of clinical trials of gene-based therapy. The first-in-human results from ocular subretinal gene augmentation therapy in *RPE65*-LCA were reported from three patients each in nearly contemporaneous Phase I/II clinical trials about 12 years ago (Cideciyan et al., 2008; Bainbridge et al., 2008; Maguire et al., 2008; Hauswirth et al., 2008). There was safety; AEs were attributable to the ocular surgery. Efficacy in most *RPE65*-LCA trials has been in rod photoreceptor-mediated vision in the region of the subretinal injection. Visual acuity improvement to a level that was clearly from cone photoreceptors has been lacking (Jacobson et al., 2012; Maguire et al., 2019; Pennesi et al., 2018). The form of LCA caused by *CEP290* mutations showed an adequate safety profile from a gene-based intravitreal therapy in Phase I/II (Cideciyan et al., 2019). In contrast to *RPE65*-LCA, the visual improvement in *CEP290*-LCA was all cone mediated with prominent visual acuity gain; this was consistent with the early loss of rod structure and function and retained central-foveal cone photoreceptors in this disorder.

After a decade of gene therapy clinical trials, clinicians and scientists working in this nascent field of treatments of rare and incurable genetic retinal disorders have few successes to claim (Garafalo et al., 2020). The results of the initial cohort of our Phase I/II *GUCY2D*-LCA subretinal gene augmentation therapy trial brings the total of "successes" (safety and visual improvement) to three forms of LCA, all representing different molecular mechanisms (Garafalo et al., 2020). How do we explain the efficacy signals in these patients in terms of rod and cone vision? Function-structure relationships in this severe retinal disease established *GUCYD*-LCA as having potential for both rod and cone visual improvement (Cideciyan and Jacobson, 2019; Jacobson et al., 2017b; Garafalo et al., 2020). P1 had a long-standing foveal loss of photoreceptors, but the remainder of the macula and surrounding retina was intact; there was no expectation of foveal cone improvement, based on the central retinal pathology. Visual acuity was severely impaired in both eyes at baseline, and there were no data trends suggesting consistent improvement in the post-operative period. The macular injection, however, would be expected to transduce the residual parafoveal cone and rod photoreceptors. Rod photoreceptor function improved by ~1 log unit in the treated eye both by perceptual and objective measures. Outside of the foveal region, cone structure is not able to be quantified independent of rods. So, whether or not there were surviving parafoveal cones to transduce is unknown.

P2 had measurably decreased foveal ONL thickness at baseline but not to the degree of the defect in P1. Baseline visual acuity of 1.25 logMAR did not change after treatment. Consistent with the lack of all catalytic activity from both alleles, only rod function was measurable and baseline acuity likely originated from rods (Jacobson et al., 2013). The superior retinal injection site would not test any hypothesis about transducing and improving visual acuity of central cones. Rod photoreceptor-mediated vision, however, did improve. The lesser degree of perceptual improvement than in P1 may be due to the lesser volume of vector-gene able to be surgically delivered (Table 1), although ~0.8 l.u. is still a substantial increase.

P3 had normal foveal ONL thickness and received a macular subretinal injection. The visual acuity at baseline of 1.27 logMAR improved to 0.92 logMAR and persisted near this level for the subsequent 9 months; the ~0.3 logMAR change (3 ETDRS lines) has been considered a clinically meaningful endpoint for ocular clinical trials (Sieving et al., 2006). The caveat is that, having chosen the worse eye (by acuity) to treat, this significant change from baseline does not improve central vision to a level considered definitively to be mediated by L/M (long/medium wavelength-sensitive) cone photoreceptors (Hecht, 1927; Lamb, 2016; Foote et al., 2018). Increased understanding of the photoreceptor basis of P3's acuity came with chromatic light-adapted sensitivity measures across the central retina, which showed partially retained cone function consistent with remnant catalytic activity from one of the two alleles (Jacobson et al., 2013). In contrast to

the untreated eye, which did not change throughout the trial, the treated eye improved in cone-mediated sensitivity after treatment. The improved acuity in P3 can be considered due to increased cone photoreceptor-mediated function. Of interest, there was also some evidence of an increment in perceptual rod function within this retinal area.

Were such results expected from proof-of-concept research in murine models that led to the clinical trial? Human GUCY2D-LCA, caused by the deficiency of RetGC1 (Jacobson et al., 2013), does not fully match a phenotype in the RetGC1 knockout murine model (Yang et al., 1995). Just like a human retina that has two RETGC isozymes (Lowe et al., 1995), a murine retina also has the two guanylyl cyclases, RetGC1 and RetGC2 (respectively, coded by *Gucy2e* and *Gucy2f* genes) (Garbers, 1999; Yang et al., 1995, 1996). However, a mouse RETGC1 knockout model (Yang et al., 1999) serves mainly as a model for cone photoreceptor therapy (Boye, 2014), because rod activity in the RetGC1-deficient mice, albeit strongly reduced, remains well detectable by ERG, whereas cone activity is completely missing (Yang et al., 1999). AAV-mediated gene augmentation indicated restoration of cone-mediated function and visual behavior in RetGC1 knockout mice (Boye et al., 2011, 2013; Mihelec et al., 2011). Cone function in human retina could in theory be positively affected. The potential for restored rod function was realized because of the proof-of-concept studies conducted in mice that lacked both RetGC1 and RetGC2 (Boye, 2014; Baehr et al., 2007; Boye et al., 2013).

In a mouse model lacking both RetGC1 and RetGC2, photoreceptors degenerate (Baehr et al., 2007), whereas rods lacking only RetGC1 survive while cones become diminished in numbers (Yang et al., 1999). RetGC2 is an ancillary enzyme in mouse rods (Peshenko et al., 2011; Olshevskaya et al., 2012) and is almost undetectable in cones (Baehr et al., 2007; Xu et al., 2013). The contribution of RetGC1 and RetGC2 in human rod and cone physiology remains unclear, but RetGC1 evidently very strongly dominates both, because the lack of RetGC1 catalytic activity (Figure 1) incapacitates rod and cone vision in patients with LCA. However, some mutations that inactivate RetGC1 (Peshenko et al., 2020) selectively affect rod but not cone vision (Stunkel et al., 2018). One of the possible explanations for that paradoxical phenotype is that, in some individuals, RetGC2 strongly contributes to the cone function. Hence, the efficacy of gene augmentation therapy in GUCY2D-LCA could be potentially influenced by the content of RetGC2 in photoreceptors.

In conclusion, there is evidence of both safety and efficacy in this first-in-human subretinal gene therapy for GUCY2D-LCA. The sample size is small and this was not a placebo-controlled trial, but that has been the case in all early phases of gene-based orphan retinal disease trials to date. There was significantly improved rod function, and in one patient, cone function also improved at this dose, the lowest intended for the trial. This bodes well, efficacy-wise, for future cohorts in the treatment of this severe childhood-onset photoreceptor disease.

Limitations of study

This interim report is limited by the number of patients and the duration of the follow-up period. The clinical trial is ongoing, and more patients will be enrolled; the three patients who are described here will also continue to be followed per the study protocol, and future measures of safety and efficacy will be made at subsequent study visits.

Resource availability

Lead contact

Requests for additional information can be directed toward the lead contact, Samuel G. Jacobson, MD, PhD (jacobsos@pennmedicine.upenn.edu).

Material availability

All materials that were generated and data that were generated are included in the manuscript. The GUCY2D coding sequence used in the generation of the vector can be viewed with the following accession information: GenBank NM_000180.4.

Data and code availability

All data are published in this manuscript and supplement; additional requests for data can be made by contacting the lead contact.

REFERENCES

Baehr, W., Karan, S., Maeda, T., Luo, D.G., Li, S., Bronson, J.D., Watt, C.B., Yau, K.W., Frederick, J.M., and Palczewski, K. (2007). The function of guanylate cyclase 1 and guanylate cyclase 2 in rod and cone photoreceptors. J. Biol. Chem. *282*, 8837–8847.

Bailey, I.L., and Lovie-Kitchin, J.E. (2013). Visual acuity testing. From the laboratory to the clinic. Vis. Res. *90*, 2–9.

Bainbridge, J.W., Smith, A.J., Barker, S.S., Robbie, S., Henderson, R., Balaggan, K., Viswanathan, A., Holder, G.E., Stockman, A., Tyler, N., et al. (2008). Effect of gene therapy on visual function in Leber's congenital amaurosis. N. Eng. J. Med. *358*, 2231–2239.

Boye, S.E. (2014). Leber congenital amaurosis caused by mutations in *GUCY2D*. Cold Spring Harb. Perspect. Med. *5*, a017350.

Boye, S.L., Conlon, T., Erger, K., Ryals, R., Neeley, A., Cossette, T., Pang, J., Dyka, F.M., Hauswirth, W.W., and Boye, S.E. (2011). Long-term preservation of cone photoreceptors and restoration of cone function by gene therapy in the guanylate cyclase-1 knockout (GC1KO) mouse. Invest. Ophthalmol. Vis. Sci. *52*, 7098–7108.

Boye, S.L., Peshenko, I.V., Huang, W.C., Min, S.H., McDoom, I., Kay, C.N., Liu, X., Dyka, F.M., Foster, T.C., Umino, Y., et al. (2013). AAV-mediated gene therapy in the guanylate cyclase (RETGC1/RETGC2) double knockout mouse model of leber congenital amaurosis. Hum. Gene Ther. *24*, 189–202.

Cideciyan, A.V., and Jacobson, S.G. (2019). Leber congenital amaurosis: potential for improvement of vision. Invest. Ophthalmol. Vis. Sci. *60*, 1680–1695.

Cideciyan, A.V., Aleman, T.S., Jacobson, S.G., Khanna, H., Sumaroka, A., Aguirre, G.K., Schwartz, S.B., Windsor, E.A., He, S., Chang, B., et al. (2007). Centrosomal-ciliary gene CEP290/NPHP6 mutations result in blindness with unexpected sparing of photoreceptors and visual brain: implications for therapy of Leber congenital amaurosis. Hum. Mutat. *28*, 1074–1083.

Cideciyan, A.V., Aleman, T.S., Boye, S.L., Schwartz, S.B., Kaushal, S., Roman, A.J., Pang, J.J., Sumaroka, A., Windsor, E.A., Wilson, J.M., et al. (2008). Human gene therapy for RPE65 isomerase deficiency activates the retinoid cycle of vision but with slow rod kinetics. Proc. Natl. Acad. Sci. U S A *105*, 15112–15117.

Cideciyan, A.V., Hauswirth, W.W., Aleman, T.S., Kaushal, S., Schwartz, S.B., Boye, S.L., Windsor, E.M., Conlon, T.J., Sumaroka, A., Roman, A.J., et al. (2009). Vision 1 year after gene therapy for Leber's congenital amaurosis. N. Engl. J. Med. *361*, 725–727.

Cideciyan, A.V., Rachel, R.A., Aleman, T.S., Swider, M., Schwartz, S.B., Sumaroka, A., Roman, A.J., Stone, E.M., Jacobson, S.G., and Swaroop,

A. (2011). Cone photoreceptors are the main targets for gene therapy of NPHP5 (IQCB1) or NPHP6 (CEP290) blindness: generation of an all-cone Nphp6 hypomorph mouse that mimics the human retinal ciliopathy. Hum. Mol. Genet. *20*, 1411–1423.

Cideciyan, A.V., Jacobson, S.G., Drack, A.V., Ho, A.C., Charng, J., Garafalo, A.V., Roman, A.J., Sumaroka, A., Han, I.C., Hochstedler, M.D., et al. (2019). Effect of an intravitreal antisense oligonucleotide on vision in Leber congenital amaurosis due to a photoreceptor cilium defect. Nat. Med. *25*, 225–228.

Csaky, K.G., Richman, E.A., and Ferris, F.L., 3rd. (2008). Report from the NEI/FDA ophthalmic clinical trial design and endpoints symposium. Invest. Ophthalmol. Vis. Sci. *49*, 479–489.

Dizhoor, A.M., Lowe, D.G., Olshevskaya, E.V., Laura, R.P., and Hurley, J.B. (1994). The human photoreceptor membrane guanylyl cyclase, RetGC, is present in outer segments and is regulated by calcium and a soluble activator. Neuron *12*, 1345–1352.

Dizhoor, A.M., Olshevskaya, E.V., and Peshenko, I.V. (2010). Mg^{2+}/Ca^{2+} cation binding cycle of guanylyl cyclase activating proteins(GCAPs): role in regulation of photoreceptor guanylyl cyclase. Mol. Cell. Biochem. *334*, 117–124.

Ebrey, T., and Koutalos, Y. (2001). Vertebrate photoreceptors. Prog. Retin. Eye Res. *20*, 49–94.

Ferris, F.L., 3rd, Kassoff, A., Bresnick, G.H., and Bailey, I. (1982). New visual acuity charts for clinical research. Am. J. Ophthalmol. 94, 91–96.

Foote, K.G., Loumou, P., Griffin, S., Qin, J., Ratnam, K., Porco, T.C., Roorda, A., and Duncan, J.L. (2018). Relationship between foveal cone structure and visual acuity measured with adaptive optics scanning laser ophthalmoscopy in retinal degeneration. Invest. Ophthalmol. Vis. Sci. 59, 3385–3393.

Garafalo, A.V., Cideciyan, A.V., Héon, E., Sheplock, R., Pearson, A., WeiYang Yu, C., Sumaroka, A., Aguirre, G.D., and Jacobson, S.G. (2020). Progress in treating inherited retinal diseases: early subretinal gene therapy clinical trials and candidates for future initiatives. Prog. Retin. Eye Res. 77, 100827.

Garbers, D.L. (1999). The guanylyl cyclase receptors. Methods 19, 477–484.

Hanein, S., Perrault, I., Gerber, S., Tanguy, G., Barbet, F., Ducroq, D., Calvas, P., Dollfus, H., Hamel, C., Lopponen, T., et al. (2004). Leber congenital amaurosis: comprehensive survey of the genetic heterogeneity, refinement of the clinical definition, and genotype-phenotype correlations as a strategy for molecular diagnosis. Hum. Mutat. 23, 306–317.

Hauswirth, W.W., Aleman, T.S., Kaushal, S., Cideciyan, A.V., Schwartz, S.B., Wang, L., Conlon, T.J., Boye, S.L., Flotte, T.R., Byrne, B.J., and Jacobson, S.G. (2008). Treatment of Leber congenital amaurosis due to RPE65 mutations by ocular subretinal injection of adeno-associated virus gene vector: short-term results of a phase I trial. Hum. Gene Ther. 19, 979–990.

Hecht, S. (1927). A quantitative basis for the relation between visual acuity and illumination. Proc. Natl. Acad. Sci. U S A 13, 569–574.

den Hollander, A.I., Roepman, R., Koenekoop, R.K., and Cremers, F.P. (2008). Leber congenital amaurosis: genes, proteins and disease mechanisms. Prog. Retin. Eye Res. 27, 391–419.

Jacobson, S.G., Cideciyan, A.V., Ratnakaram, R., Heon, E., Schwartz, S.B., Roman, A.J., Peden, M.C., Aleman, T.S., Boye, S.L., Sumaroka, A., et al. (2012). Gene therapy for Leber congenital amaurosis caused by RPE65 mutations: safety and efficacy in 15 children and adults followed up to 3 years. Arch. Ophthalmol. 130, 9–24.

Jacobson, S.G., Cideciyan, A.V., Peshenko, I.V., Sumaroka, A., Olshevskaya, E.V., Cao, L., Schwartz, S.B., Roman, A.J., Olivares, M.B., Sadigh, S., et al. (2013). Determining consequences of retinal membrane guanylyl cyclase (RetGC1) deficiency in human Leber congenital amaurosis en route to therapy: residual cone-photoreceptor vision correlates with biochemical properties of the mutants. Hum. Mol. Genet. 22, 168–183.

Jacobson, S.G., McGuigan, D.B., 3rd, Sumaroka, A., Roman, A.J., Gruzensky, M.L., Sheplock, R., Palma, J., Schwartz, S.B., Aleman, T.S., and Cideciyan, A.V. (2016). Complexity of the class B phenotype in autosomal dominant retinitis pigmentosa due to rhodopsin mutations. Invest. Ophthalmol. Vis. Sci. 57, 4847–4858.

Jacobson, S.G., Cideciyan, A.V., Sumaroka, A., Roman, A.J., Charng, J., Lu, M., Choi, W.,

Sheplock, R., Swider, M., Kosyk, M.S., et al. (2017a). Outcome measures for clinical trials of Leber congenital amaurosis caused by the intronic mutation in the CEP290 gene. Invest. Ophthalmol. Vis. Sci. 58, 2609–2622.

Jacobson, S.G., Cideciyan, A.V., Sumaroka, A., Roman, A.J., Charng, J., Lu, M., Choudhury, S., Schwartz, S.B., Heon, E., Fishman, G.A., and Boye, S.L. (2017b). Defining outcomes for clinical trials of Leber congenital amaurosis caused by GUCY2D mutations. Am. J. Ophthalmol. 177, 44–57.

Kumaran, N., Pennesi, M.E., Yang, P., Trzupek, K.M., Schlecter, C., Moore, A.T., Weleber, R.G., and Michaelides, M. (2018). Leber congenital amaurosis/early-onset severe retinal dystrophy overview. In GeneReviews® [Internet], M.P. Adam, H.H. Ardinger, and R.A. Pagon, et al., eds. (University of Washington, Seattle), pp. 1993–2020.

Lamb, T.D. (2016). Why rods and cones? Eye 30, 179–185.

Li, Y., Wang, H., Peng, J., Gibbs, R.A., Lewis, R.A., Lupski, J.R., Mardon, G., and Chen, R. (2009). Mutation survey of known LCA genes and loci in the Saudi Arabian population. Invest. Ophthalmol. Vis. Sci. 50, 1336–1343. https://doi.org/10.1167/iovs.08-2589.

Lowe, D.G., Dizhoor, A.M., Liu, K., Gu, Q., Spencer, M., Laura, R., Lu, L., and Hurley, J.B. (1995). Cloning and expression of a second photoreceptor-specific membrane retina guanylyl cyclase (RetGC), RetGC-2. Proc. Natl. Acad. Sci. U S A 92, 5535–5539.

Luo, X., Cideciyan, A.V., Iannaccone, A., Roman, A.J., Ditta, L.C., Jennings, B.J., Yatsenko, S.A., Sheplock, R., Sumaroka, A., Swider, M., et al. (2015). Blue cone monochromacy: visual function and efficacy outcome measures for clinical trials. PLoS One 10, e0125700.

Maguire, A.M., Simonelli, F., Pierce, E.A., Pugh, E., Jr., Mingozzi, F., Bennicelli, J., Banfi, S., Marshall, K.A., Testa, F., Surace, E.M., et al. (2008). Safety and efficacy of gene transfer for Leber's congenital amaurosis. N. Eng. J. Med. 358, 2240–2248.

Maguire, A.M., Russell, S., Wellman, J.A., Chung, D.C., Yu, Z.F., Tillman, A., Wittes, J., Pappas, J., Elci, O., Marshall, K.A., et al. (2019). Efficacy, safety, and durability of Voretigene Neparvovec-rzyl in RPE65 mutation-associated inherited retinal dystrophy: results of phase 1 and 3 trials. Ophthalmol 126, 1273–1285.

Matsui, R., Cideciyan, A.V., Schwartz, S.B., Sumaroka, A., Roman, A.J., Swider, M., Huang, W.C., Sheplock, R., and Jacobson, S.G. (2015). Molecular heterogeneity within the clinical diagnosis of pericentral retinal degeneration. Invest. Ophthalmol. Vis. Sci. 56, 6007–6018.

Mihelec, M., Pearson, R.A., Robbie, S.J., Buch, P.K., Azam, S.A., Bainbridge, J.W., Smith, A.J., and Ali, R.R. (2011). Long-term preservation of cones and improvement in visual function following gene therapy in a mouse model of Leber congenital amaurosis caused by guanylate cyclase-1 deficiency. Hum. Gene Ther. 22, 1179–1190.

Olshevskaya, E.V., Peshenko, I.V., Savchenko, A.B., and Dizhoor, A.M. (2012). Retinal guanylyl cyclase isozyme 1 is the preferential in vivo target for constitutively active GCAP1 mutants causing congenital degeneration of photoreceptors. J. Neurosci. 32, 7208–7217.

Palczewski, K., Subbaraya, I., Gorczyca, W.A., Helekar, B.S., Ruiz, C.C., Ohguro, H., Huang, J., Zhao, X., Crabb, J.W., Johnson, R.S., et al. (1994). Molecular cloning and characterization of retinal photoreceptor guanylyl cyclase-activating protein. Neuron 13, 395–404.

Pennesi, M.E., Weleber, R.G., Yang, P., Whitebirch, C., Thean, B., Flotte, T.R., Humphries, M., Chegarnov, E., Beasley, K.N., Stout, J.T., and Chulay, J.D. (2018). Results at 5 years after gene therapy for RPE65-deficient retinal dystrophy. Hum. Gene Ther. 29, 1428–1437.

Perrault, I., Rozet, J.M., Calvas, P., Gerber, S., Camuzat, A., Dollfus, H., Châtelin, S., Souied, E., Ghazi, I., Leowski, C., et al. (1996). Retinal-specific guanylate cyclase gene mutations in Leber's congenital amaurosis. Nat. Genet. 14, 461–464.

Peshenko, I.V., Olshevskaya, E.V., Savchenko, A.B., Karan, S., Palczewski, K., Baehr, W., and Dizhoor, A.M. (2011). Enzymatic properties and regulation of the native isozymes of retinal membrane guanylyl cyclase (RetGC) from mouse photoreceptors. Biochemistry 50, 5590–5600.

Peshenko, I.V., Olshevskaya, E.V., and Dizhoor, A.M. (2020). GUCY2D mutations in retinal guanylyl cyclase 1 provide biochemical reasons for dominant cone-rod dystrophy but not for stationary night blindness [published online ahead of print]. J. Biol. Chem. 295, 18301–18315.

Roman, A.J., Cideciyan, A.V., Aleman, T.S., and Jacobson, S.G. (2007). Full-field stimulus testing (FST) to quantify visual perception in severely blind candidates for treatment trials. Physiol. Meas. 28, N51–N56.

Roman, A.J., Schwartz, S.B., Aleman, T.S., Cideciyan, A.V., Chico, J.D., Windsor, E.A., Gardner, L.M., Ying, G.S., Smilko, E.E., Maguire, M.G., and Jacobson, S.G. (2005). Quantifying rod photoreceptor-mediated vision in retinal degenerations: dark-adapted thresholds as outcome measures. Exp. Eye Res. 80, 259–272.

Sharon, D., Wimberg, H., Kinarty, Y., and Koch, K.W. (2018). Genotype-functional-phenotype correlations in photoreceptor guanylate cyclase (GC-E) encoded by GUCY2D. Prog. Retin. Eye Res. 63, 69–91.

Sieving, P.A., Caruso, R.C., Tao, W., Coleman, H.R., Thompson, D.J., Fullmer, K.R., and Bush, R.A. (2006). Ciliary neurotrophic factor (CNTF) for human retinal degeneration: phase I trial of CNTF delivered by encapsulated cell intraocular implants. Proc. Natl. Acad. Sci. U S A 103, 3896–3901.

Stunkel, M.L., Brodie, S.E., Cideciyan, A.V., Pfeifer, W.L., Kennedy, E.L., Stone, E.M., Jacobson, S.G., and Drack, A.V. (2018). Expanded retinal disease spectrum associated with autosomal recessive mutations in GUCY2D. Am. J. Ophthalmol. 190, 58–68.

Vinberg, F., Peshenko, I.V., Chen, J., Dizhoor, A.M., and Kefalov, V.J. (2018). Guanylate cyclase-activating protein 2 contributes to

phototransduction and light adaptation in mouse cone photoreceptors. J. Biol. Chem. *293*, 7457–7465.

Xu, J., Morris, L., Thapa, A., Ma, H., Michalakis, S., Biel, M., Baehr, W., Peshenko, I.V., Dizhoor, A.M., and Ding, X.Q. (2013). cGMP accumulation causes photoreceptor degeneration in CNG channel deficiency: evidence of cGMP

cytotoxicity independently of enhanced CNG channel function. J. Neurosci. *33*, 14939–14948.

Yang, R.B., Foster, D.C., Garbers, D.L., and Fulle, H.J. (1995). Two membrane forms of guanylyl cyclase found in the eye. Proc. Natl. Acad. Sci. U S A *92*, 602–606.

Yang, R.B., Fülle, H.J., and Garbers, D.L. (1996). Chromosomal localization and genomic

organization of genes encoding guanylyl cyclase receptors expressed in olfactory sensory neurons and retina. Genomics *31*, 367–372.

Yang, R.B., Robinson, S.W., Xiong, W.H., Yau, K.W., Birch, D.G., and Garbers, D.L. (1999). Disruption of a retinal guanylyl cyclase gene leads to cone-specific dystrophy and paradoxical rod behavior. J. Neurosci. *19*, 5889–5897.

Supplemental information
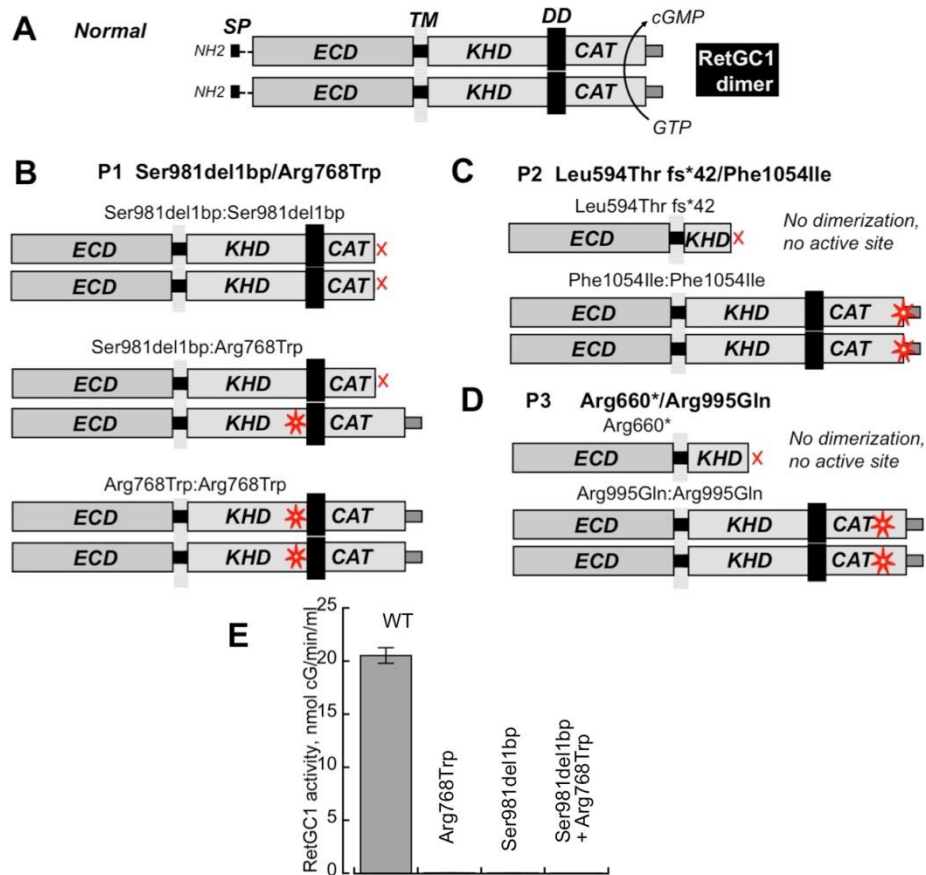
Safety and improved efficacy signals

following gene therapy in childhood blindness caused by *GUCY2D*

mutations

Samuel G. Jacobson, Artur V. Cideciyan, Allen C. Ho, Igor V. Peshenko, Alexandra V. Garafalo, Alejandro J. Roman, Alexander Sumaroka, Vivian Wu, Arun K. Krishnan, Rebecca Sheplock, Sanford L. Boye, Alexander M. Dizhoor, and Shannon E. Boye

Supplemental Information

Figure S1: RetGC1 dimer combinations that can be produced by the *GUCY2D* alleles in the patients. Related to Figure 1. (A) The schematics of the normal RetGC1 primary structure and its catalytically active dimer; SP- the removable N-terminal signal peptide, ECD- extracellular domain, TM-transmembrane fragment, KHD- kinase homology domain, DD- dimerization domain, CAT- catalytic domain (Garbers, 1999). RetGC1 becomes catalytically active only as a dimer (Yang et al., 1997), when the catalytic domains of the two subunits form a common active site converting GTP to cGMP (Liu et l., 1997). (B) In P1 (Table 1), the Ser981del1bp frame-shift truncates the C-terminal portion of the catalytic domain, but the products of both alleles harbor the normal dimerization domain and hence can produces homodimers Ser981del1bp:Ser981del1bp or Arg768Trp:Arg768Trp and a heterodimer Ser981del1bp: Arg768Trp. (C) One of the two LCA alleles in the patient P2, Phe1054Ile, retains both the dimerization domain and the catalytic domain. The Leu594Thr fs42* RetGC1 coded by the second LCA allele has a truncated kinase homology domain and lacks both the dimerization and the catalytic domains altogether. Hence, this RetGC1 mutant cannot create the active site and likely fails to dimerize, neither as a homodimer nor as a heterodimer. (D). In P3, also only one of the two *GUCY2D* LCA alleles, Arg995Gln, can form a homodimer Arg995Gln: Arg995Gln. The second allele product, Arg660*, is truncated in the middle of the kinase homology domain, hence it lacks the dimerization and the catalytic domains and would be unable to dimerize and form the active site. *Asterisks* indicate position of the mutations in the primary structure of the polypeptides. (E) HEK293 cells co-transfected with RetGC1 cDNAs coding for the two LCA allele products in P1 do not produce active enzyme. RetGC activity was assayed in the presence of 20 µM GCAP1.
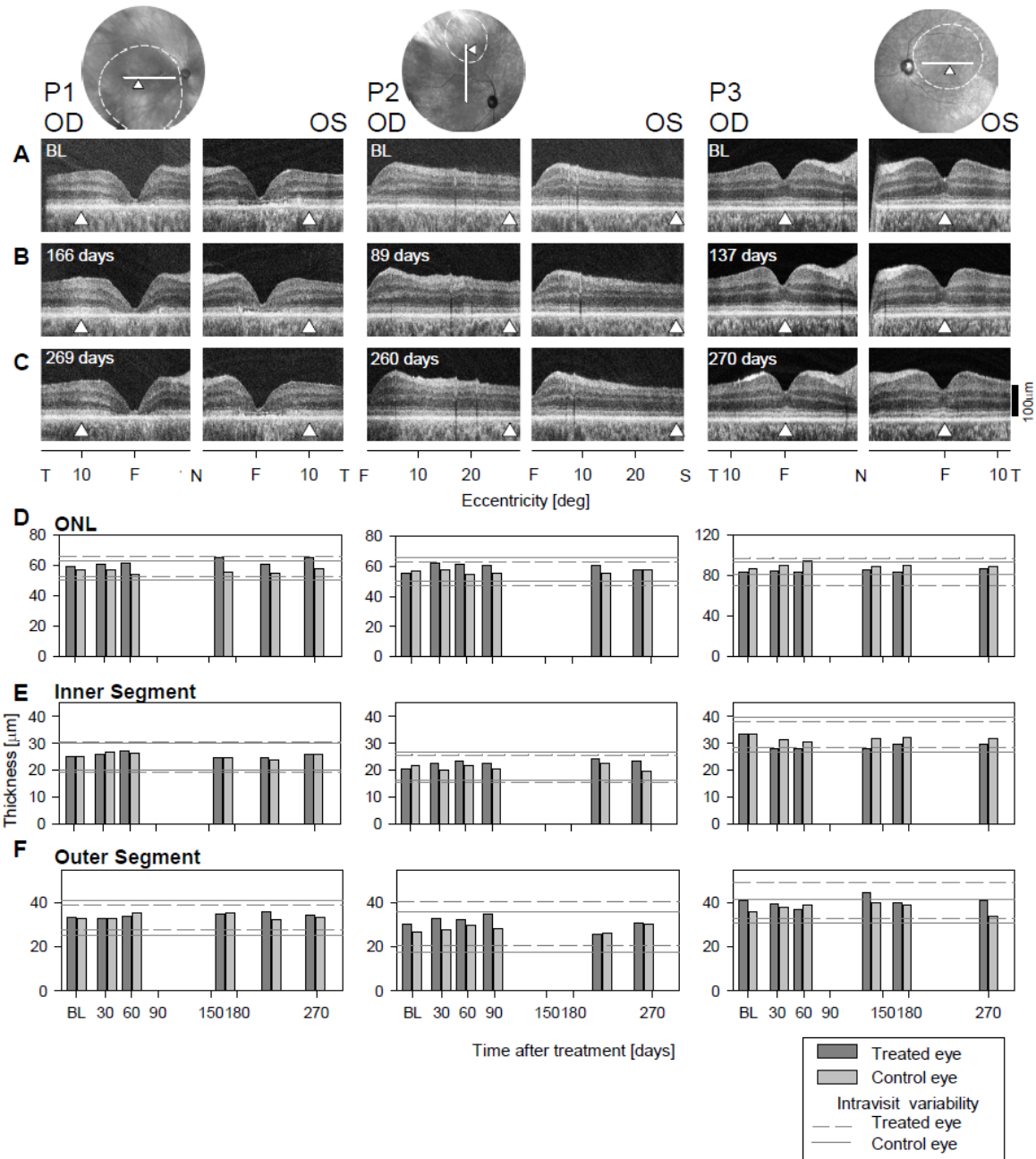
Figure S2: Quantitation of the photoreceptor sublayers in the patients at Baseline and post-operative visits spanning 9 months. Related to Figure 2. Representative OCT scans at (A) Baseline, (B) visit 3 and (C) visit 5 after the surgery. Above the scans are near-infrared fundus images of the treated eyes with site of bleb (injection location) marked (delimited by dashed line). White lines on the fundus images represent the position of the OCT scan. The white up-triangle along the line on the fundus images and on the eccentricity axes of the scans show the location selected for quantitation of photoreceptor layers in D-F. (D) Bar graphs are a measurement of ONL (outer nuclear layer), (E) IS (inner segment), and (F) OS (outer segment) thickness at baseline and at five visits after surgery for the treated eye (dark gray bar) and control eye (light gray bar). Dashed and solid black lines delimit intravisit variability in the treated and untreated eye, respectively.
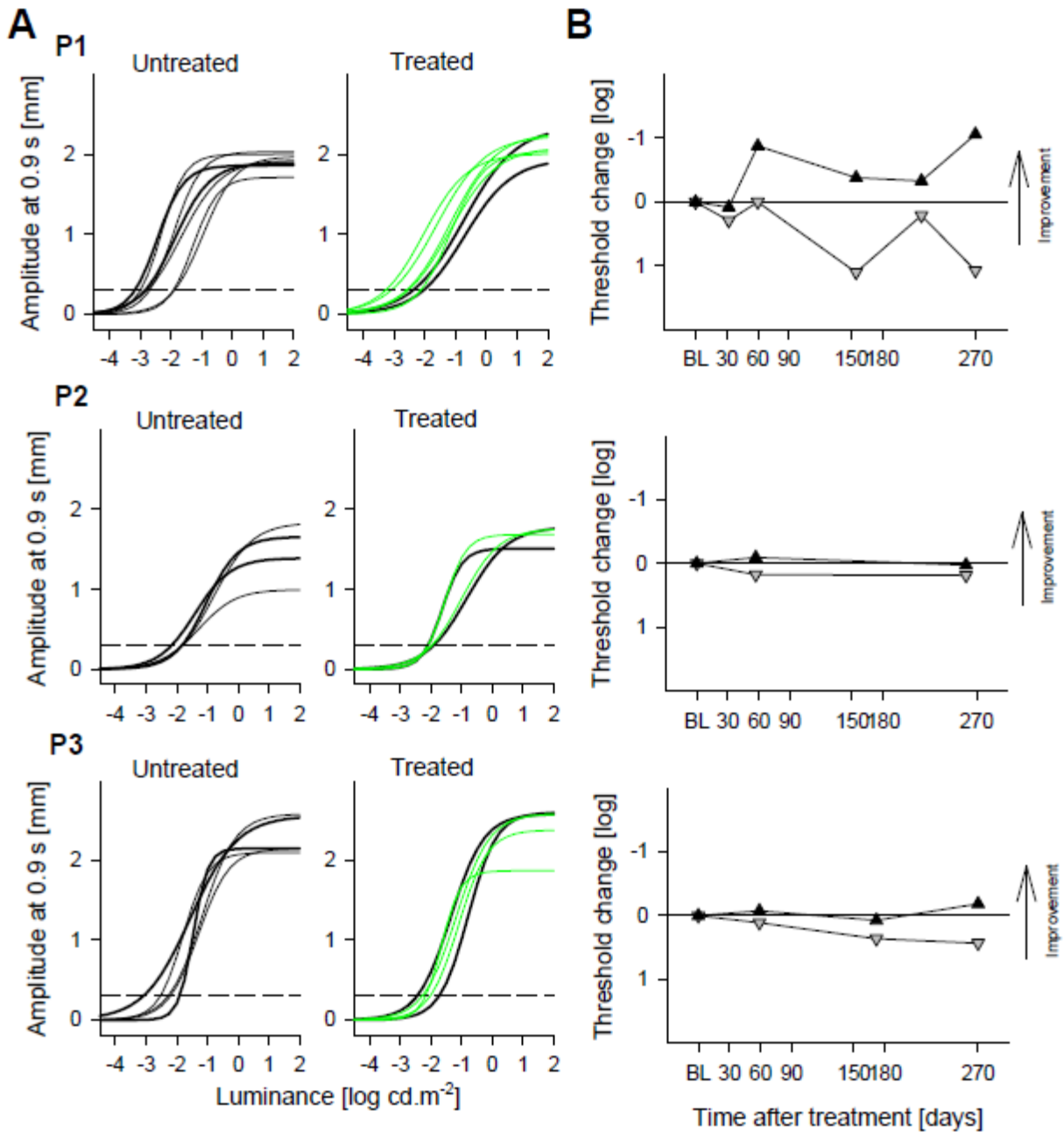
Figure S3: Dark-adapted pupillary light reflexes in the patients at baseline and post-operative visits spanning 9 months. Related to Figure 3. (A) Non-linear functions best fit to pupillary response amplitudes measured at 0.9 s after the start of 1 s long red stimuli over a 6 log unit dynamic range of luminances presented to dark-adapted eyes. Thicker lines represent the pre-treatment time points, thinner black and green lines represent the post-treatment time points in untreated and treated eyes, respectively. Horizontal dashed lines demarcate criterion amplitude of 0.3 mm used to define response thresholds. (B) Change in response threshold from average pre-treatment values. Black up-triangles are treated eyes; gray down-triangles are untreated control eyes.
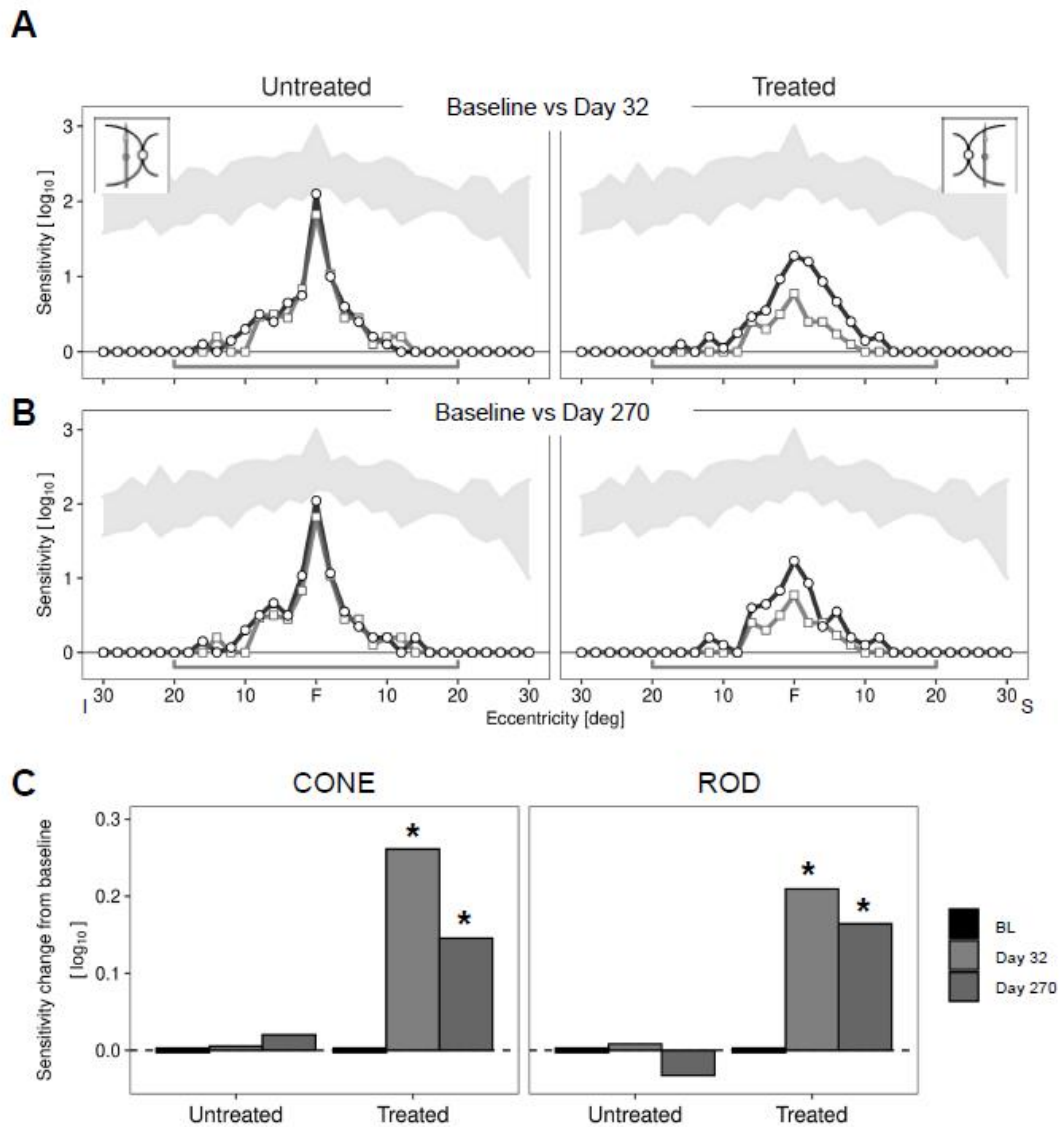
Figure S4. Cone and rod function at baseline and post-op visits in P3. Related to Figure 4. (A) Light-adapted (600 nm stimulus) sensitivity profiles across the vertical meridian in untreated (left panel) and treated (right panel) eyes at baseline (symbols connected by gray lines) and post-op day 32 (symbols connected by black lines) visits in P3. Normal data, shaded area ±2 SD from mean. (B) Light-adapted profiles comparing baseline and 270 days post-op visit data in P3. Plots and symbols as in A. F, fixation; I, inferior, S, superior visual field; bracket below profiles represents the data averaged and plotted for the horizontal profile. Data from vertical profiles within the central 40° were also averaged and plotted in C. (C) Sensitivity changes (average of horizontal and vertical profiles across central 40°) are shown as bars for untreated and treated eyes. Left panel: light-adapted 600 nm data. Right panel: dark-adapted 500 nm data. All dark-adapted 500 nm sensitivities were rod-mediated. Asterisks on the treated eye bars indicate when interocular differences with respect to baseline were significantly different than zero (α=0.05, eye/visit interaction term in a linear model).
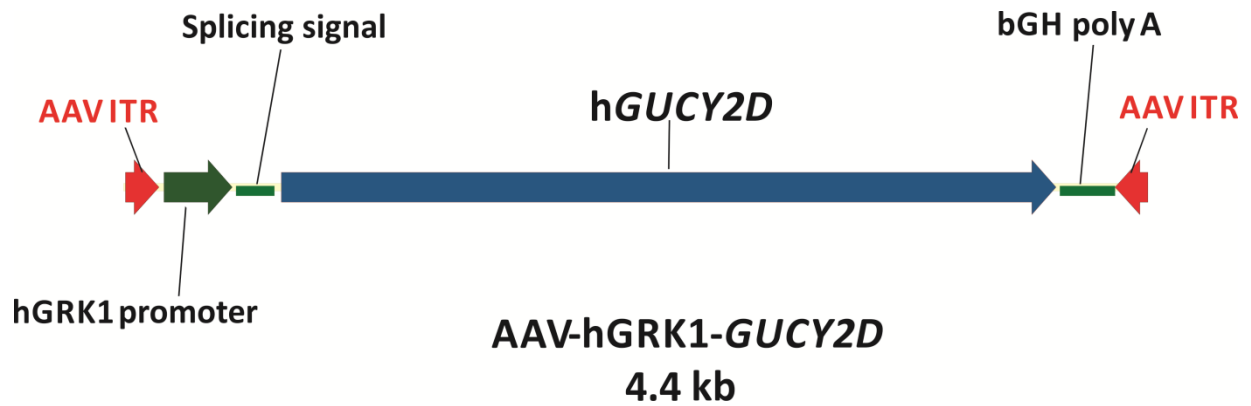
Figure S5. Schematic diagram of the gene therapy vector. Related to Table 1. AAV ITR= Adeno-associated virus type 2 inverted terminal repeat; hGRK1= human rhodopsin promoters (Khani et al. 2007); splicing signal= SV40 splice donor, splice acceptor sites; h*GUCY2D*= full coding region of human guanylate cyclase 1; bGH polyA= bovine growth hormone poly-adenylation signal

Table S1. Schedule of Study Visits. Related to Table 1.

Visit:	Pre-therapy		Days											Years	
	Screening	Baseline	1	2	3	4-7	8-14	30	60	90	180	270	365	1.5	2
Informed consent/assent	■														
LCA genetic testing (if needed)	■														
Medical and surgical history	■														
Physical examination	■														
Electrocardiogram	■														
Pregnancy test	■	■						■							
Vital signs measurements	■	■	■	■	■	■	■	■	■	■	■	■	■	■	■
Study agent administration			■												
Hematology, chemistry, urinalysis	■	■				■		■				■			■
Ophthalmic exam	■	■		■	■	■	■	■	■	■	■	■	■	■	■
Best corrected visual acuity	■	■		■	■	■	■	■	■	■	■	■	■	■	■
Full-field stimulus testing	■	■			■		■	■	■	■	■	■	■	■	■
Fundus imaging	■	■		■	■			■	■	■	■	■	■	■	■
Optical coherence tomography	■							■	■	■	■	■	■	■	■
Pupillometry	■	■						■	■	■	■	■	■	■	■
Oculomotor instability	■	■						■	■	■	■	■	■	■	■
Questionnaire		■						■		■	■		■	■	■
Adverse event recording	■	■	■	■	■	■	■	■	■	■	■	■	■	■	■

Note: Electroretinography (ERG) was not performed due to the facts that ERGs are non-detectable in most of these patients and nystagmus can make recording and interpretation difficult.
Note: Dosing and cohort information is as follows:
Part A: Dose Escalation
Part B: Patients will be treated with the maximum tolerated dose or the maximum administered dose based on Part A.
Total enrollment will be approximately 15 patients.
Cohorts 1-4: patients ≥18 years old
Cohort 5: patients ≥6 years old and <18 years old

Table S2. Ocular Adverse Events. Related to Table 1.

Description of adverse event	No. of patients experiencing event (n=3)	Intensity
Discomfort	3	Mild
Subconjunctival hemorrhage	3	Mild
Hypotony	2	Mild
Vitreous cells	1	Mild
Steroid induced ocular hypertension	1	Mild
Retinal hole	1	Mild

TRANSPARENT METHODS

REGULATORY APPROVALS AND OVERSIGHT

The open label clinical trial, registered on ClinicalTrials.gov (NCT03920007), is being performed at Scheie Eye Institute of the University of Pennsylvania (UP) and Wills Eye Institute (WEI) of Thomas Jefferson University Hospital. The trial protocol was reviewed and accepted by the United States Food and Drug Administration (Investigational New Drug application IND 18659). Approvals were obtained from the Institutional Review Boards and Institutional Biosafety Committees of UP and WEI. A Data and Safety Monitoring Committee oversees the trial. The tenets of the Declaration of Helsinki were followed. Informed consent was obtained from the participants.

METHOD DETAILS

The gene therapy vector (Figure S5). The AAV5-*GUCY2D* vector comprises the human rhodopsin kinase promoter (Khani et al.,2007), followed by the human *GUCY2D* coding sequence (accession # NM_000180.4) and a poly adenylation signal derived from bovine growth hormone, all flanked by AAV2 inverted terminal repeats and contained within AAV5 capsid. Virus was manufactured under good manufacturing practices (GMP) and purified as previously described (Nass et al., 2017).

Molecular diagnosis. *GUCY2D* mutations in the patients were certified by CLIA (Clinical Laboratory Improvement Amendments) approved molecular laboratories.

Surgical procedure. Three port pars plana vitrectomy (core and peripheral; intravitreal triamcinolone was used) was performed and a posterior vitreous detachment was induced. The subretinal injection needle (41-gauge) was guided to the region around the superior vascular arcades and the surgeon placed a retinotomy within the boundaries of the arcades (MicroDose Injection Kit, MedOne Surgical, Inc). The study drug was injected slowly to form a subretinal bleb in the macula. After study drug administration, the fundus was examined for any retinal breaks. A partial air-fluid exchange was performed. Sclerotomy sites were inspected for leakage and no sclerotomies required suturing. A normal intraocular pressure was verified. Triamcinalone acetonide (20mg in 0.5mL) was injected periocularly. Patients took oral prednisone (dose at investigator discretion, but a maximum dose of 1mg/kg up to 80mg) daily starting the day before surgery through the second day following surgery. Prednisolone 1% drops and trimethoprim and polymyxin B drops were also administered to the study eye four times per day starting the day after surgery through day 9.

Safety evaluations. Ocular safety was assessed with standard eye examinations at two baseline visits, and daily for the first 14 days after treatment and at 5 visits post-treatment spanning 9 months. OCT was performed to assess retinal integrity during the pre- and post-treatment evaluations. Systemic safety at baseline and post-operative visits was assessed with physical examinations, routine hematology, serum chemistry, coagulation parameters, and urinalysis. To document fundus appearance, photographs (using an infrared camera to avoid excess visible light exposure) were taken at baseline and at post-treatment visits.

Visual function and retinal structure. Visual function was measured using ETDRS visual acuity (Ferris et al., 1982) in two of the patients. One patient's severe visual disability precluded use of standard ETDRS methods and the Berkeley Rudimentary Vision Test was used (Bailey et al., 2012). Dark-adapted chromatic full-field stimulus testing (FST) was performed with short- (blue) and long-wavelength (red) stimuli (200 ms duration) (Jacobson et al., 2017; Roman et al., 2007) Dark-adapted transient pupillary light reflexes were performed with red (1 s duration) full-field stimuli (Charng et al., 2017; Krishnan et al.,

2020). In each patient, baseline data were available from screening and baseline pre-treatment visits; post-treatment data were obtained up to 9 months after surgery.

For FST, the dependent variable was visual threshold expressed in $\log_{10}$ phot-cd m^{-2}. Multiple measurements (median n=18) were obtained for both conditions (blue and red) at each visit. Linear models were used separately for each condition with treatment-by-visit interactions as fixed effects. The treatment factor had two levels (treated and untreated eyes), and the visit factor had 5 or 6 levels (baseline and subsequent study visits). The visits where the interactions were significant (α=0.05) are marked with asterisks (Figure 3), indicating where the interocular difference was significantly different than the one at baseline, and 95% confidence intervals for the visit means (±2 SEM) are shown in brackets. In these instances the treated eye showed better relative performance than the untreated.

For visual acuity, ETDRS and tumbling E charts read from left-to-right, and right-to-left were used in each eye to attempt to minimize learning effects. 5 to 8 independent acuity estimates were obtained pre-treatment on different days, 2 to 3 estimates were obtained post-treatment. Comparisons were performed between all available pre-treatment and post-treatment samples at month 9 (two sample, 2-tailed t-test, α=0.05). The dependent variable was the Minimum Angle of Resolution expressed in $\log_{10}$ (logMAR). Levels of change from baseline in logMAR and in ETDRS equivalent lines (no change, 3 lines improvement or decrease, these corresponding to ±0.3 logMAR changes; Figure 4) enabled comparison with other clinical trials of retinal degenerations that used ETDRS as an outcome (Sieving et al., 2006).

Chromatic light-adapted (600 nm) and dark-adapted (500 and 650 nm) sensitivity profiles were performed with a modified automated perimeter and using published methods (Roman et al., 2005; Matsui et al., 2015; Jacobson et al., 1986). A comparison of sensitivity changes from baseline (averaged over horizontal and vertical profiles within the central 40^0, Fig. 5) was performed as described for FST, with visit factor having three levels (baseline, Day 32 and Day 270), separately for 500- and 600 nm data.

Retinal structure was assessed by cross-sectional imaging using spectral domain optical coherence tomography (OCT; RTVue-100, Optovue Inc., Fremont, CA) (Jacobson et al., 2013; Jacobson et al., 2017; Sumaroka et al., 2016). The OCT images were recorded routinely in the macula and extramacular retina of each eye of the patients. Scans at post-operative visits were compared by observation with those at baseline; measurements were also made of outer nuclear layer (ONL), inner segment (IS) and outer segment (OS) thicknesses. Post-acquisition processing of OCT data was performed with custom programs (MATLAB Release, 2020, MathWork, Natick, MA). Three 30°-wide B-scans composed of 1,019 A-scans or longitudinal reflectivity profiles (LRPs) were selected from both eyes of each subject at each visit. All scans were aligned by straightening the major hyperreflective signal believed to originate near the interface between the basal aspect of the retinal pigment epithelium and Bruch's membrane; the foveola was identified manually as the maximum depression. Quantitative measurements of retinal laminae were performed after reduction of lateral sampling density by averaging seven neighbors (sampling bins were 0.2 degrees). Three retinal layers were identified and manually segmented with a computer-assisted algorithm using LRPs. The hyposcattering ONL was defined between the hyperscattering outer plexiform layer (OPL) and the maximum of hyperscattering outer limiting membrane (OLM); the foveal ONL thickness was defined as the distance between the internal limiting membrane and outer limiting membrane; IS length was defined as the distance between OLM peak and peak of IS/OS; and OS as distance between IS/OS peak and inner boundaries of RPE. From this segmentation, thickness of ONL, IS and OS layers were extracted. At selected eccentricities, single value of layer thickness represents the average of 3 measurements along the horizontal scan at 0.2-degree increments centered at the foveal pit, or 5 measurements with the same increment centered 10° temporal and 28° superiorly.

Biochemical studies. Human RetGC1 was expressed in HEK293 cells from a modified pRCCMV vector containing RetGC1 cDNA transfected using calcium-phosphate precipitation method and the membranes containing RetGC1 were isolated as previously described in detail (Peshenko et al., 2015). Mutations

were introduced in RetGC1 cDNA using 'splicing by overlap extension' site-directed mutagenesis *in vitro* or by using chemically synthesized fragments harboring the desired mutations to replace portions in the RetGC1 cDNA that harbored new restriction endonuclease sites not altering the encoded protein sequence (Peshenko et al., 2020). Recombinant human GCAP1 was expressed and purified as described (Peshenko et al, 2008) with modifications (Peshenko et al., 2019). Guanylyl cyclase activity was assayed using [alpha-^{32}P]GTP as a substrate (Peshenko et al., 2020; Peshenko et al., 2004) in the presence of 2 mM EGTA and 10 mM $MgCl_2$. [32P]cGMP was quantified using thin-layer chromatography and liquid scintillation counting as described previously (Peshenko et al., 2020).

Schedule of Study Visits. The schedule of study visits and the study activities performed at each visit are summarized in Table S1.

SUPPLEMENTAL REFERENCES

Bailey, I.L., Jackson, A.J., Minto, H., Greer, R.B., and Chu, M.A. (2012). The Berkeley rudimentary vision test. Optom. Vis. Sci. *89,* 1257-1264.

Charng, J., Jacobson, S.G., Heon, E., Roman, A.J., McGuigan, D.B., Sheplock, R., Kosyk, M.S., Swider, M., and Cideciyan, A.V. (2017). Pupillary light reflexes in severe photoreceptor blindness isolate the melanopic component of intrinsically photosensitive retinal ganglion cells. Invest. Ophthalmol. Vis. Sci. *58*, 3215-3224.

Jacobson, S.G., Voigt, W.J., Parel, J.M., Apáthy, P.P., Nghiem-Phu, L., Myers, S.W., and Patella, V. M. (1986). Automated light- and dark-adapted perimetry for evaluating retinitis pigmentosa. Ophthalmology *93*, 1604–1611.

Khani, S.C., Pawlyk, B.S., Bulgakov, O.V., Kasperek, E., Young, J.E., Adamian, M., Sun, X., Smith, A.J., Ali, R.R. and Li, T. (2007). AAV-mediated expression targeting of rod and cone photoreceptors with a human rhodopsin kinase promoter. Invest. Ophthalmol. Vis. Sci. *48*, 3954–3961.

Krishnan, A.K., Jacobson, S.G., Roman, A.J., Iyer, B.S., Garafalo, A.V., Héon, E., Cideciyan, A.V. (2020) Transient pupillary light reflex in CEP290- or NPHP5-associated Leber congenital amaurosis: latency as a potential outcome measure of cone function. Vision Res. *168*, 53-63.

Liu, Y., Ruoho, A.E., Rao, V.D., and Hurley, J.H. (1997). Catalytic mechanism of the adenylyl and guanylyl cyclases: modeling and mutational analysis. Proc. Natl. Acad. Sci. USA. *94,* 13414-13419.

Nass, S.A., Mattingly, M.A., Woodcock, D.A., Burnham, B.L., Ardinger, J.A., Osmond, S.E., Frederick, A.M., Scaria, A., Cheng, S.H. and O'Riordan, C.R. (2017). Universal method for the purification of recombinant AAV vectors of differing serotypes. Mol. Ther. Methods Clin. Dev. *9*, 33–46.

Peshenko, I.V., Moiseyev, G.P., Olshevskaya, E.V. and Dizhoor, A.M. (2004). Factors that determine Ca2+ sensitivity of photoreceptor guanylyl cyclase. Kinetic analysis of the interaction between the Ca2+-bound and the Ca2+-free guanylyl cyclase activating proteins (GCAPs) and recombinant photoreceptor guanylyl cyclase 1 (RetGC-1). Biochemistry *43*, 13796–13804.

Peshenko, I.V., Olshevskaya, E.V., and Dizhoor, A.M. (2008). Binding of guanylyl cyclase activating protein 1(GCAP1) to retinal guanylyl cyclase (RetGC1): the role of individual EF-hands. J. Biol. Chem. *283*, 21747-21757.

Peshenko, I.V., Olshevskaya, E.V., and Dizhoor, A.M. (2015). Evaluating the role of retinal membrane guanylyl cyclase 1 (RetGC1) domains in binding guanylyl cyclase-activating proteins(gCAPs). J. Biol. Chem. *290*, 6913-6924.

Peshenko, I.V., Cideciyan, A.V., Sumaroka, A., Olshevskaya, E.V.,Scholten, A., Abbas, S., Koch, K.W., Jacobson, S.G., and Dizhoor, A.M. (2019). A Gly86Arg mutation in the calcium-sensor protein GCAP1 alters regulation of retinal guanylyl cyclase and causes dominant cone-rod degeneration. J. Biol. Chem. *294*, 3476-3488.

Sumaroka, A., Matsui, R., Cideciyan, A.V., McGuigan, D.B.,3rd, Sheplock, R., Schwartz, S.B., and Jacobson, S.G. (2016). Outer retinal changes including the ellipsoid zone band in Usher syndrome 1B due to MYO7A mutations. Invest. Ophthalmol. Vis. Sci. *57*, OCT253-261.

Yang, R.B., and Garbers, D.L. (1997). Two eye guanylyl cyclases are expressed in the same photoreceptor cells and form homomers in preference to heteromers. J. Biol. Chem. *272*, 13738-13742.